PERGAMON

Journal of Structural Geology 26 (2003) 1021–1036

JOURNAL OF STRUCTURAL GEOLOGY

www.elsevier.com/locate/jsg

Palinspastic reconstruction of structure maps: an automated finite element approach with heterogeneous strain

John A. Dunbar[a,*], Richard W. Cook[b]

[a]*Department of Geology, Baylor University, PO 97354, Waco, TX 76798, USA*
[b]*Shell International Oil Company, Houston, TX, USA*

Received 27 January 2002; accepted 12 September 2002

Abstract

Existing methods for the palinspastic reconstruction of structure maps do not adequately account for heterogeneous rock strain and hence cannot accurately treat features such as fault terminations and non-cylindrical folds. We propose a new finite element formulation of the map reconstruction problem that treats such features explicitly. In this approach, a model of the map surface, with internal openings that honor the topology of the fault-gap network, is constructed of triangular finite elements. Both model building and reconstruction algorithms are guided by rules relating fault-gap topology to the kinematics of fault motion and are fully automated. We represent the total strain as the sum of a prescribed component of locally homogeneous simple shear and a minimum amount of heterogeneous residual strain. The region within which a particular orientation of simple shear is treated as homogenous can be as small as an individual element or as large as the entire map. For residual strain calculations, we treat the map surface as a hyperelastic membrane. A globally optimum reconstruction is found that unfolds the map while faithfully honoring assigned strain mechanisms, closes fault gaps without overlap or gap and imparts the least possible residual strain in the restored surface. The amount and distribution of the residual strain serves as a diagnostic tool for identifying mapping errors. The method can be used to reconstruct maps offset by any number of faults that terminate, branch and offset each other in arbitrarily complex ways.

Keywords: Map reconstruction; Structure map topology; Finite element method

1. Introduction

Convenient and reasonably accurate methods for the palinspastic reconstruction of cross-sections have been known for several decades (e.g. Dahlstrom, 1969; Gibbs 1983; Rowan and Kligfield, 1989). Cross-section reconstruction is used to test the consistency of structural interpretations with geometric, kinematic and geological rules expected to govern the growth of the structure. In their general forms, the rules governing palinspastic reconstruction apply to three dimensions. Further restrictions are required to reduce the reconstruction procedure to a set of steps that can be applied to cross-sections using graphical methods (Gibbs, 1983). Chief among these restrictions are the plane-strain assumption and the assumption of homogenous strain within fault blocks. The first assumption implies that folds are cylindrical and faults are pure dip-slip. The second assumption precludes the accurate treatment of heterogeneous strain associated with terminating faults. Together, these assumptions allow the restored shape of each fault block to be determined independently. Complex structures involving many faults can then be restored in a fault-block-by-fault-block recursive manner. However, misfit between fault blocks tends to accumulate as successive blocks are restored, so that the final blocks require a disproportionate share of the deformation. Even so, for most well chosen cross-sections, problems associated with non-cylindrical folding, out of the plane motion, terminating faults and solution order are relatively minor. As first described, cross-section reconstruction methods were intended for manual implementation (Dahlstrom, 1969; Gibbs, 1983; Rowan and Kligfield, 1989). More recently, computer-aided implementations of the same procedures have become available that make their routine use practical (e.g. Morretti and Larrere, 1989; Worrall and Snelson, 1989; Schultz-Ela, 1991; Erickson et al., 2000).

* Corresponding author.
E-mail address: john_dunbar@baylor.edu (J.A. Dunbar).

0191-8141/03/$ - see front matter © 2002 Elsevier Science Ltd. All rights reserved.
PII: S0191-8141(02)00154-2

However, these computer-aided implementations have the same limitations as the graphical methods upon which they are based.

Petroleum structural traps are inherently three-dimensional in nature. Hence, there is interest in extending reconstruction methods to test the validity of structure maps developed in petroleum exploration. However, problems associated with heterogeneous strain and solution order that produce minor errors in most cross-section reconstructions become a significant source of error in map reconstructions. Early approaches to map reconstruction amounted to little more than the application of the cross-section rules to the horizontal plane (Barr, 1985). In Barr's method, the effects of folding are removed by an optional cylindrical roll-over correction to the surface area of each fault block. Then fault gaps are closed one-at-a-time by applying simple shear in the horizontal plane in an assigned direction. Gratier et al. (1991), Gratier and Guiller (1993) and Rouby et al. (1993, 2000) describe progressive improvements on a method that addresses the problems of non-cylindrical folding and heterogeneous strain. In their approach, complex maps with terminating faults are first subdivided into separate fault blocks along artificial breaks and then the fault blocks are further subdivided into triangular elements. The reconstruction is performed in stages. Initially, the restored shape of each triangle is computed independently, assuming flexural slip or simple shear (Rouby et al., 2000). This allows for local variations in strain. The restored positions of the triangles within a fault block are then automatically computed by a recursive least-squares algorithm such that there is the least possible overlap and gap between adjacent restored triangles. The corner points of neighboring triangles are then shifted so they coincide. This cosmetically restores the continuity between adjacent triangles, but at the cost of the accuracy of local area preservation. Next, the fault blocks are fit back together one-at-a-time, again with the least square overlap and gap. Although this method represents a significant step forward, the problems associated with solution-order artifacts and the accurate treatment of terminating faults still remain to be resolved.

In this paper, we describe a map reconstruction method that extends the ideas of Rouby et al. (2000) in two important ways. First, we develop a more complete geometric model that faithfully represents both the geometry and topology of complexly faulted horizon surfaces. Rather than breaking maps into separate fault blocks, fault terminations and complexly shaped internal fault gaps are treated explicitly. The geologic significance of points and curves that define the fault gaps are automatically recognized and recorded during model construction. This allows the reconstruction to also be fully automated. The second extension of the ideas of Rouby et al. (2000) is to treat map reconstruction as a global optimization problem. In this way, solution-order artifacts are avoided. We seek a reconstruction in which fault gaps are closed, while strict continuity is maintained between the triangular elements defining the map surface and the deformation of the surface is removed according to a prescribed simple shear mechanism. To the extent possible, this is done without additional distortion of the surface. Heterogeneous strain around fault terminations and at mismatching fault cutoff curves is accommodated using a large-strain elasticity formulation. We use the amount and distribution of the heterogeneous strain as a diagnostic tool to judge the validity of the original map.

2. Horizon model

2.1. Representing the topology of faulted map surfaces

The key to reconstructing faulted maps by an automatic algorithm is to start with a geometric model that faithfully represents not only the shape of faulted horizons, but also the topology and geologic attributes. In general, geologic horizons are dissected by arbitrarily complex gap networks (Fig. 1). The gaps are bounded by horizon cutoff curves, which define the intersections between the horizon and crosscutting surfaces. The cutoff curves join at their ends to form closed loops, except where they artificially terminate at map edges. Depending on the type of the crosscutting surfaces, cutoff curves have different geologic significance. They may define the intersection between the horizon and faults, salt or unconformities. Fault-cutoff curves may define either the footwall or hanging wall side of a fault gap. Individual cutoff curves are broken into separate segments where different horizon-cutting surfaces intersect.

As a first step in the model building process, we manually identify the type of crossing surface that produced each cutoff curve (Fig. 1b). We then digitize individual cutoff curve segments in a counter-clockwise direction around the gap network and order segments within curves in a counter-clockwise sequence. Curve direction is used by the model building algorithm to discriminate between gap areas and areas that are part of the map surface. The horizon cutoff network is resampled into line elements that are linked in closed counter-clockwise loops around openings in the map surface. A surface model composed of triangular elements is automatically generated using a tessellation algorithm similar to those described by Green and Sibson (1978), Deljouie-Rakhshandeh (1990) and Jin and Wiberg (1990) (Fig. 2a). The algorithm fills the regions between the map boundary and the cutoff curve network with triangular elements that have sides that coincide with the linear elements of the cutoff network, the map boundary or are completely internal to the map surface (Fig. 2b). The vertical coordinates of the triangle nodes are constrained to honor horizon elevation data or digitized contours in a least-squares sense.

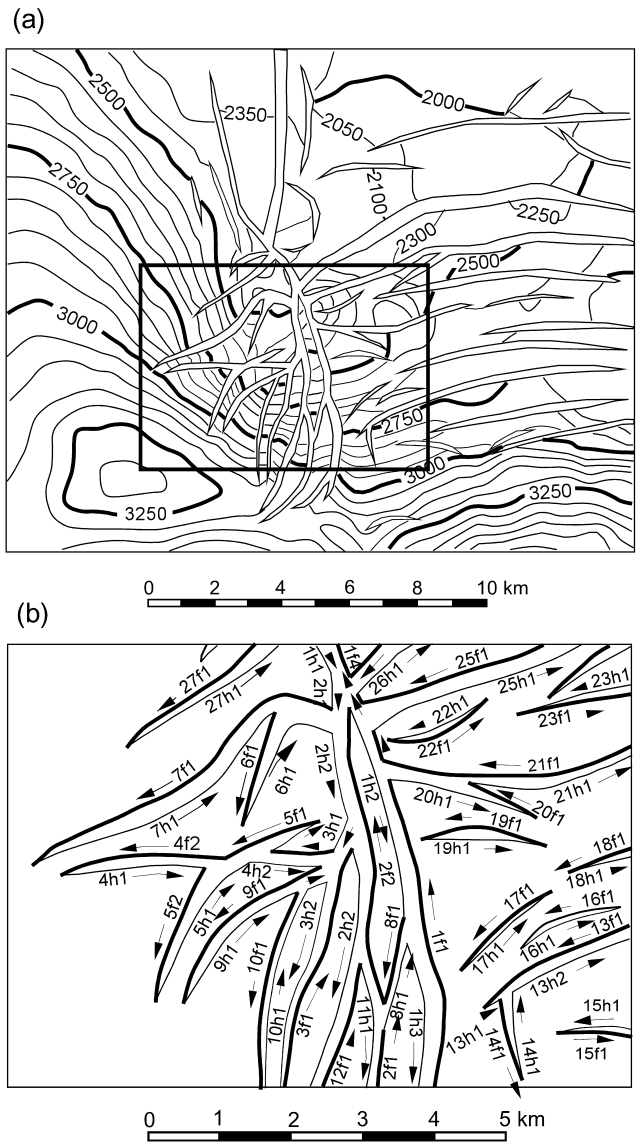

Fig. 1. Topology of faulted and folded horizon maps. (a) Example subsurface horizon map constructed from well data and two-dimensional seismic data. Horizon cutoff curves bounding fault gaps form closed loops, except at artificial openings at map edges. Depth contours are in meters. (b) Enlargement showing digitizing and naming conventions for cutoff curve segments. Cutoff curves are digitized in a counter-clockwise direction and divided into separate hanging wall and footwall cutoff curves. Fault branches further subdivide cutoff curves into segments, which are also ordered in a counter-clockwise direction around the gaps.

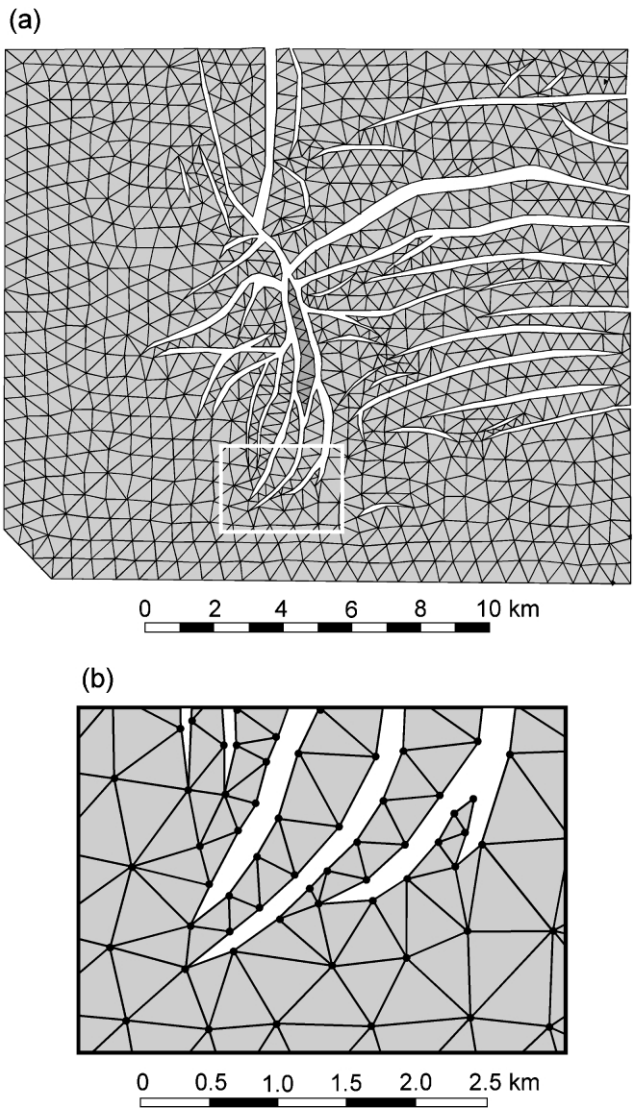

Fig. 2. Finite element model of a faulted and folded horizon surface. (a) Automatic tessellation of the map surface honors both the geometry and topology of the fault gap network of the map shown in Fig. 1. (b) Corner nodes are shared between adjacent triangles and curve segments along horizon cutoff curves, insuring continuity in the restored map.

2.2. Kinematic rules governing horizon cutoff curves

Recognizing the kinematic significance of different kinds of cutoff-curve termination points is fundamental to the automatic map reconstruction algorithm. Non-artificial terminations of fault-cutoff curve segments occur in only four kinematically distinct types (Fig. 3). The model-building algorithm analyzes the linkages between cutoff curves to classify each cutoff-curve termination point as one of these four types. Intersections at the ends of the first and last segments in fault-cutoff curves correspond to tip points, if the intersecting curves meet at an acute angle about the gap (Fig. 3a) and low-angle or synthetic branch points, if they form an obtuse angle about the gap (Fig. 3b). Intersections involving one internal curve segment end and one first or last segment end correspond to high-angle or antithetic branch points (Fig. 3c). Intersections between two internal segment ends are faulted-fault points (Fig. 3d).

The different types of fault-gap termination points behave differently during reconstruction. Tip points are welded in the deformed configuration and remain welded in the restored configuration. Synthetic branch points are free to slide along a conjugate cutoff curve and may switch to other conjugate curves during reconstruction. Antithetic branch points and faulted-fault points each have a conjugate point on an adjacent cutoff segment that must be restored to

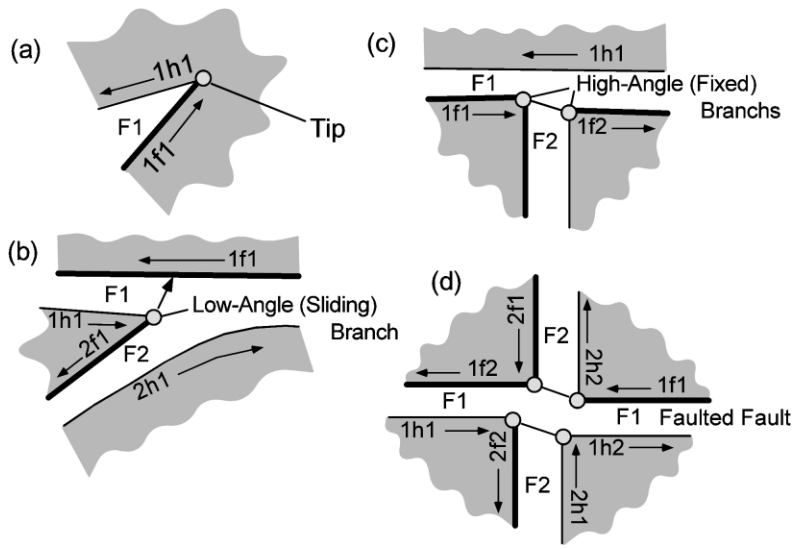

Fig. 3. Kinematic rules for horizon cutoff curve intersections. Four distinct types of intersections are possible between horizon cutoff curves, labeled (a), (b), (c), and (d). Fault-salt and fault-unconformity intersections are kinematically equivalent to high-angle branch between faults (type c).

the same location in the reconstruction. The relationship between branch points constrains the relative positions of fault blocks within the restored map. Ambiguity occurs only in instances of through-going faults that artificially cut the map into entirely separate fault blocks. In these instances, at least one pair of conjugate points must be manually identified between each fault block to resolve the ambiguity.

3. Minimum strain reconstruction

3.1. Heterogeneous strain

The goal of map reconstruction is to restore a horizon to its depositional configuration by flattening the folding and closing the fault gaps or removing fault overlaps (Fig. 4). Ideally, individual elements within the surface model could be flattened by one of a number of locally homogeneous deformation mechanisms, including vertical-simple shear, antithetic shear, synthetic shear or bed-parallel shear (Fig. 4b). However, it is generally not possible to define the deformation accurately enough such that the triangles can be restored, while also retaining continuity between adjacent triangles and closing the fault gaps. Because the true deformation kinematics are imperfectly known, it is normally necessary to relax one of these mutually exclusive kinematic requirements in order to produce a reconstruction. We take an approach in which the most constrained kinematic requirements are honored accurately and approximations are allowed to the least constrained requirement. Hence, we choose to maintain continuity between neighboring triangles and to close fault gaps accurately. In the finite element formulation, perfect continuity between elements is guaranteed by the fact that corner nodes of adjacent elements are shared. Accurate closure of fault gaps is forced through the addition of kinematic constraints that require nodes along footwall fault-cutoff curves to move to and remain in contact with the conjugate hanging wall cutoff curves. To do this it is necessary to allow a component of additional heterogeneous strain of the element shapes beyond that prescribed by the idealized strain mechanisms. We call this component ‘residual strain’ and seek a reconstruction that produces the smallest total and smoothest distribution of residual strain possible through the methods of constrained non-linear optimize (Fletcher, 1987) (Fig. 4c). This component of residual strain is not interpreted as actual rock strain, but is used as a measure of the extent to which the actual rock strain can be explained by the deformation mechanisms prescribed by the user. In this way, the minimum strain criterion is analogous to and replaces the least-squares fit criterion between adjacent triangles used in the reconstruction method of Gratier et al. (1991), Gratier and Guiller (1993) and Rouby et al. (2000). This approach makes it possible to flatten non-cylindrical folds while maintaining perfect continuity between neighboring triangles. It also makes it possible to explicitly treat faults that terminate within the map area without resorting to artificially breaking the map into separate fault blocks.

3.2. Hyperelastic membrane formulation

To produce reconstructions with the least total and smoothest distribution of residual strain, we treat residual strain using a hyperelastic membrane formulation. A membrane is a thin sheet with no bending strength, but with resistance to shape distortion (Gruttmann and Taylor, 1992). Elastic deformation has the desired property of guaranteeing the least total and the smoothest possible distribution of strain for a given set of kinematic boundary conditions. Hyperelasticity allows this to occur at large strains. This is analogous to the deformation of a thin rubber sheet. We choose this formulation, not as an approximation

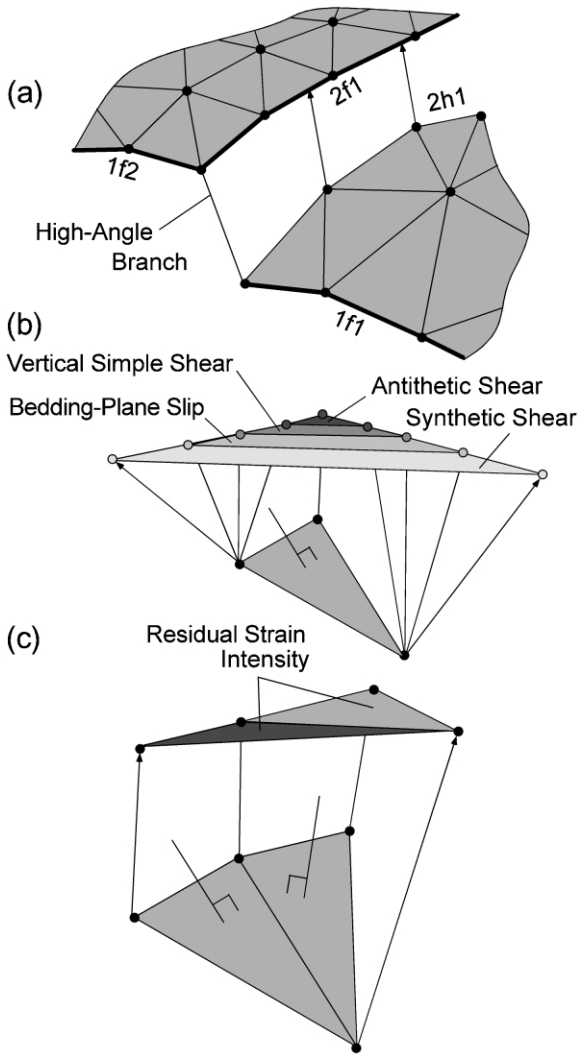

Fig. 4. Kinematic rules governing map reconstruction. (a) Fault gaps are closed by forcing contact between nodes on hanging-wall horizon cutoff curves and conjugate footwall cutoff curves. Conjugate points at high-angle fault branches are forced to coincide in the restored configuration. (b) Objective restored shapes are computed independently for each triangular element, consistent with a specified homogenous deformation mechanism. (c) The restored map is the solution to a non-linear optimization that seeks to close the fault gaps, while the elements take on their objective shapes. A solution is sought that requires the least possible residual strain. Variations in residual strain levels over the restored map are depicted in shades of gray and used to judge how well maps reconstruct.

to the actual physics of the rock deformation, but because it has the desired kinematic properties for the residual component of strain in the reconstruction problem.

The strain energy density at a point on the hyperelastic membrane is given by (Fried and Johnson, 1988; Gruttmann and Taylor, 1992):

$$W = \frac{\mu}{2}\left[B_{ii} - 2 - \ln\left(\det B_{ij}\right)\right] + \frac{\lambda}{2}\left[\det F_{ij} - 1\right]^2, \qquad (1)$$

where

$F_{ij} = \dfrac{\partial x_i}{\partial X_j}$ = the deformation gradient,

$\det F_{ij} - 1$ = the normalized area change,

$B_{ij} = F_{ki}F_{kj}$ = Green′s strain,

μ is the shear modulus, λ is Lame's constant, which is proportional to the bulk modulus, X_i is the reference ith coordinate of the point, x_i is the deformed (restored) ith coordinate of the point, i and j take on the horizontal coordinate indices 1 and 2.

In conventional continuum mechanics problems, the reference configuration of the body defined by X_i is the undeformed state. In the map reconstruction problem, we define the residual strain in terms of the distortion of the surface beyond that incurred by flattening with the assumed strain mechanism. Hence, the reference configuration of a triangle is the ideal flattened shape, rather than the present-day shape. The ideal shapes are calculated analytically by independently flattening the triangles by rotation or according to an assumed simple shear rule.

Changes to the map surface area beyond that associated with the assumed strain mechanism are not desirable. In the membrane formulation, this is equivalent to the deformation of an incompressible material. To enforce incompressibility in such materials the bulk strain term in Eq. (1) is commonly replaced by an area penalty term (Simo and Taylor, 1982). This term makes an arbitrarily large contribution or penalty to the strain energy in response to bulk strain. The objective function to be minimized is the resulting strain energy density integrated over the area of an element Ω

$$O^{e}_{\Omega} = \frac{\mu}{2}\int_{\Omega}\left[B_{ii} - 2 - \ln\left(\det B_{ij}\right)\right]\partial\Omega + P_{\Omega}\int_{\Omega}\left[\det F_{ij} - 1\right]^2\partial\Omega, \qquad (2)$$

where P_{Ω} is a penalty coefficient for element Ω, chosen such that the area is preserved to within a specified tolerance. For the reconstruction problem the shear modulus μ is also an arbitrary constant. In practice the area integrals in Eq. (2) are evaluated numerically for each element.

3.3. Kinematic constraints for unfolding and fault contact

The strain energy (Eq. (2)) occurs in response to flattening folds and closing fault gaps during reconstruction. These requirements are cast in the same form as kinematic boundary conditions between bodies in contact in conventional continuum mechanics problems. In the new reconstruction method, contact constraints applied to nodes along fault gaps replace restoration vectors assigned by the user in previous map reconstruction methods. Contact constraints differ in that they force contact, but do not restrict the point of contact or the direction of relative motion. The points of contact and directions of motion between fault blocks are found as a part of the global residual strain minimization process.

In general, map reconstructions require kinematic

constraints that force individual nodes to move to and remain in contact with the depositional surface, another node in the model, or with a specific line element within the model (Fig. 4a). Such contact constraints are enforced through the addition of penalty terms that each contributed to the global objective function when the condition is not met and vanish when the condition is met. These added contact constraint terms O^{c}_{Φ}, for contact Φ, are of the possible forms:

$O^{c}_{\Phi} = P_{\Phi}(x^{j}_{i} - V)^2$, which forces the ith coordinate of node j to restore to a specified value V,
$O^{c}_{\Phi} = P_{\Phi}(x^{j}_{i} - x^{k}_{i})^2$, which forces the ith coordinate of node j to restore to the same value as the ith coordinate of node k,
$O^{c}_{\Phi} = P_{\Phi}(Ax^{n}_{1} + Bx^{n}_{2} + C)^2$, which forces node n to restore to a position in contact with a fixed line segment defined by constant coefficients A, B, and C,
$O^{c}_{\Phi} = P_{\Phi}[A(x^{j}_{2}, x^{k}_{2})x^{n}_{1} + B(x^{j}_{1}, x^{k}_{1})x^{n}_{2} + C(x^{j}_{1}, x^{j}_{2}, x^{k}_{1}, x^{k}_{2})]^2$, which forces node n to restore to a position in contact with a line segment through nodes j and k, defined by variables coefficients $A(x^{j}_{2}, x^{k}_{2})$, $B(x^{j}_{1}, x^{k}_{1})$, and $C(x^{j}_{1}, x^{j}_{2}, x^{k}_{1}, x^{k}_{2})$.

The global objective function for the optimum reconstructed configuration is found by summing the contributions from each element objective function plus those associated with each contact constraint:

$$O^{g} = \sum_{\Omega=1}^{N^{e}} O^{e}_{\Omega} + \sum_{\Phi=1}^{N^{c}} O^{c}_{\Phi}, \tag{3}$$

where N^{e} is the number of elements in the map surface and N^{c} is the number of contact constraints required to restore the map to the depositional surface and close the fault gaps.

This casts map reconstruction as a nonlinear optimization problem. The solution is the restored configuration that minimizes the global objective function Eq. (3). To find the solution we use Galerkin's method to write Eq. (3) in terms of the positions of the triangle corner nodes within the surface model (Becker et al., 1981; Dhatt and Touzot, 1984). The optimum nodal positions are found by Newton's method. Corrections that move the model nodes from the present-day to the restored configuration are found by repeatedly solving a large sparse system of linear equations.

4. Reconstruction algorithm

The reconstruction formulation described in the previous section takes the form of a finite element solution to a continuum mechanics problem. In principle, the problem could be solved using a general-purpose finite element software package. However, this would be prohibitively labor intensive for routine use. Even if the finite element model is generated automatically, thousands of contact constraints must be assigned to reconstruct maps of moderate complexity. Nodes constrained to lie along fault cutoff curves are free to slide from line segment to line segment along the curve. During reconstruction, these contacts must be reassigned as the constrained nodes move from one target line segment to the next. For a practical implementation, we developed a special purpose finite element program with an automatic algorithm that assigns and updates these contact constraints in a geologically reasonable manner during reconstruction.

Initial contact constraints between nodes on footwall cutoff curves and line segments along conjugate hanging wall cutoff curves are not assigned by the user, but by a special initial conjugate assignment algorithm (Fig. 5). To make this contact assignment, it is only necessary to identify a valid conjugate cutoff curve to which the initial contact can be made without crossing solid parts of the map surface. This assignment can be made automatically by an algorithm that analyzes the topology of the fault gap network. The key to this algorithm is having a model data structure in which each model component has geologic type information and a record of all adjacent components. The initial assignment algorithm works on the principle that, other than for small differences in post-faulting deformation, conjugate footwall and hanging wall gaps should be equal in length. The algorithm locates an initial target line segment by summing lengths along a path around the fault gap. Footwall segments along the path are counted as positive contributions to the sum, whereas hanging wall segments are counted as negative contributions. Jumps between conjugate branch points along the path do not contribute to the sum. Starting at a contact node on the footwall cutoff, tracking proceeds from curve segment to curve segment along the footwall, until either a tip, conjugate branch or user supplied link to a hanging wall cutoff is found. Tracking continues along an arbitrary number of footwall and hanging wall curve segments until the net path length becomes zero. This establishes only the initial target assignments. During the reconstruction, the contact point is free to move along the target curve and its final position is found as part of the minimum residual strain solution.

The reconstruction process begins with the independent computation of the objective restored shape of each triangle according to the specified strain mechanisms. Given these objective shapes and initial contact constraints, a minimum residual strain solution is found by a series of Newton iterations. Once convergence is reached, a check is made to determine if the contact conditions are satisfied to within a specified tolerance. If the penalty constants for one or more contact conditions require adjustment to reach the specified tolerance, the solution is repeated. Contact conditions that are satisfied to within tolerance are solved exactly and the associated dependent degrees of freedom are algebraically eliminated from future iterations. When convergence is

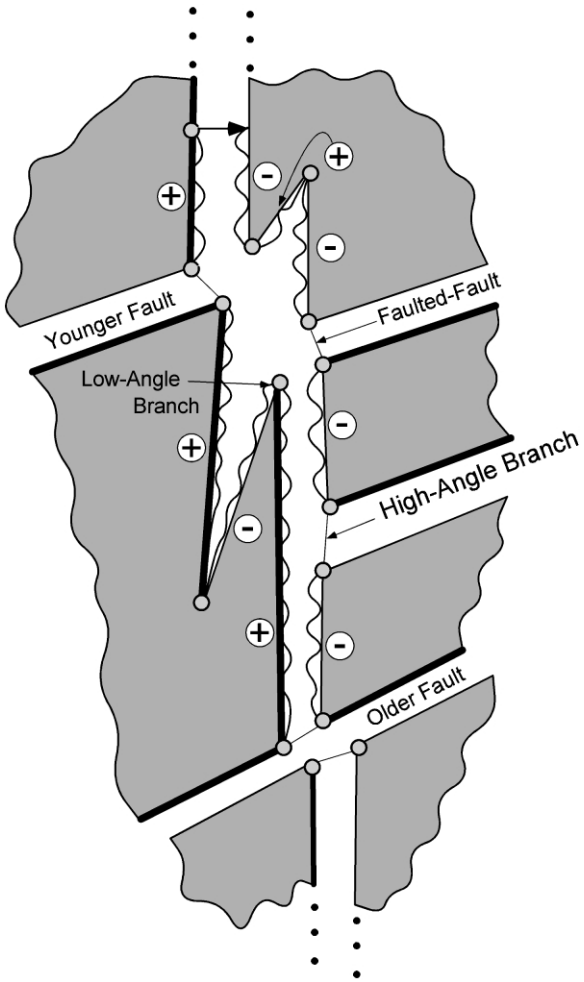

Fig. 5. Initial assignment of fault contact constraints. Estimates of fault contact positions are automatically determined for each hanging wall node by tracking along the horizon cutoff network. Lengths along footwall segments are counted as positive and lengths along hanging wall segments are counted as negative. Jumps are made between conjugate points at high-angle fault branches. Tracking continues through arbitrarily complex fault gap networks until the sum reaches zero at the point where the length of conjugate footwall and hanging wall segments match. This algorithm identifies an initial conjugate cutoff curve to which hanging wall nodes can make contact without crossing solid parts of the map surface. The position of contact is updated automatically during the reconstruction process and the target conjugate cutoff can change as hanging wall nodes slide past low-angle branch points (Fig. 6). The final position is determined as part of the global strain minimization process.

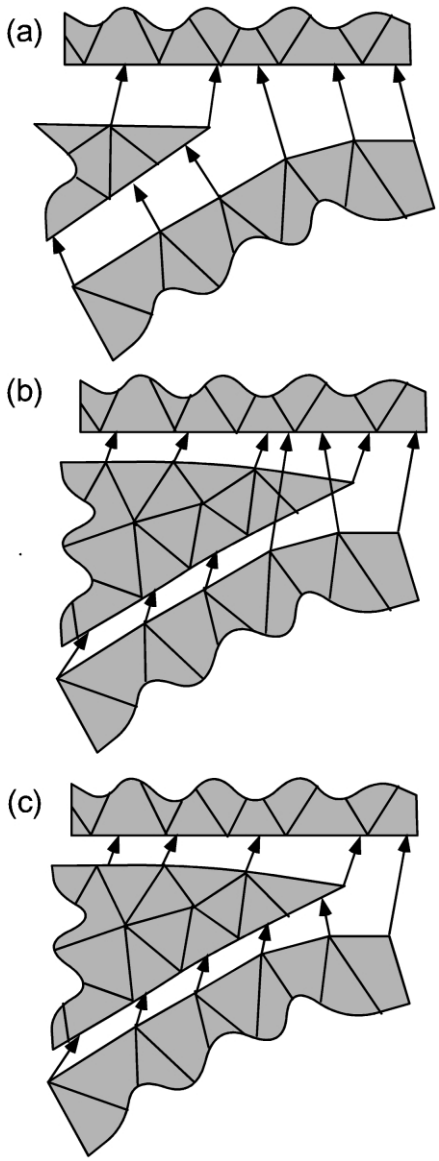

Fig. 6. Local contact node tracking. (a) During reconstruction contact nodes slide along conjugate footwall cutoff curves to reach the minimum residual strain configuration. (b) After convergence, the positions of the contact nodes are checked to see if they have moved off the end of their assigned target line segments or past a sliding branch point. (c) If they have, adjacency information is used to track the node position to a new target. In this illustration the fault gaps are exploded to show contact relationships between blocks.

reached and all constraints are satisfied, a contact tracking algorithm checks the position of the contact nodes to determine if they have moved past the end of their assigned target line segment or past a sliding branch point of another fault block (Fig. 6). New target line segments are assigned accordingly and the solution is repeated. A final solution is reached when a minimum energy configuration is found in which all constraints are satisfied to within tolerance and all contact nodes have remained on the same target from the preceding iteration. The entire solution process proceeds automatically, without user input.

5. Synthetic examples

5.1. Fault termination

To test the accuracy with which various kinematic constraints can be enforced, we consider three synthetic examples patterned after those given by Rouby et al. (2000) (Figs. 7–9). The first example illustrates the difference between a least square fit reconstruction (Fig. 7a–c) and a continuum reconstruction that minimizes residual strain

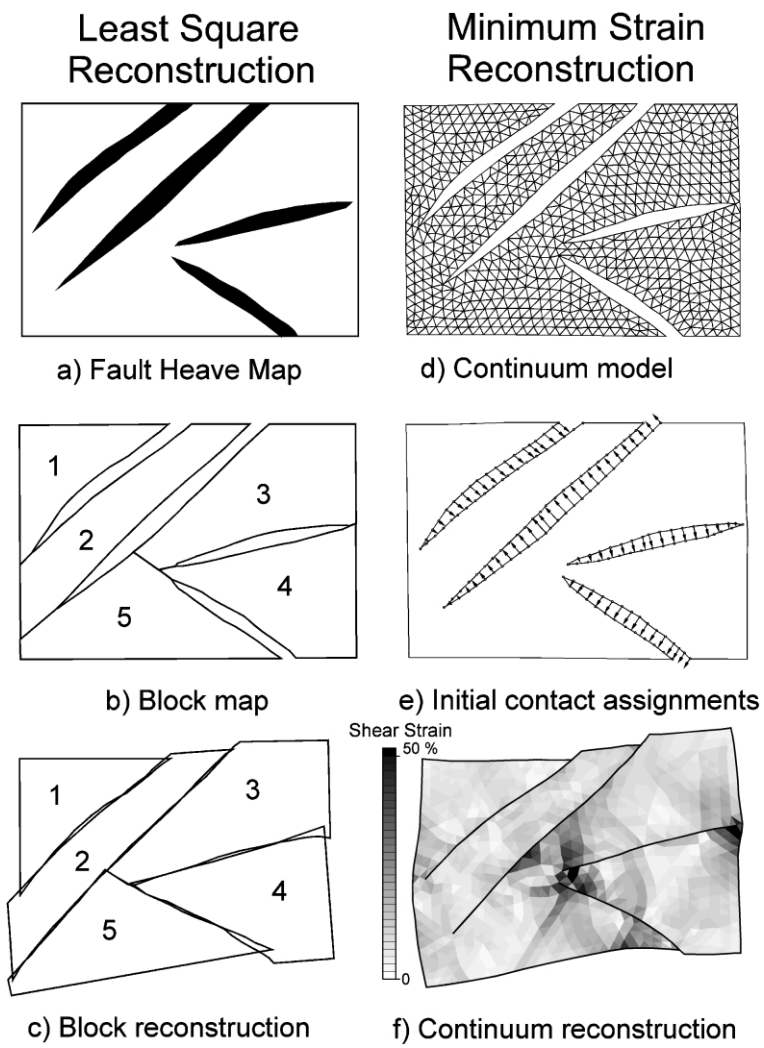

Fig. 7. Synthetic example with terminating faults. (a), (b), and (c) show the true initial configuration, the initial configuration divided into separate fault blocks, and the least square block reconstruction, respectively, after Rouby et al. (2000). (d), (e), and (f) are the continuum element model, the initial contact assignment, and the minimum residual strain reconstruction, respectively, produced by the methods described in this paper.

(Fig. 7d–f). The initial map (Fig. 7a) represents an unfolded map surface in which the fault gaps remain to be closed. In this example, the strain involved in unfolding is ignored and only the strain associated with closing fault gaps is considered. In the least square fit strategy followed by Rouby et al. (2000), the faults are each artificially extended to intersect another fault or the map edge, producing separate fault blocks (Fig. 7b). The separate fault blocks are then translated and rotated as rigid bodies, one at a time, to a restored configuration that results in the least square overlap and gap between adjacent fault blocks (Fig. 7c). No additional strain is allowed within the blocks. Reconstruction error appears as a combination of fault slip beyond tips and overlap and gap between fault blocks. In this synthetic example, the maximum slip beyond fault tip reaches 10% of the fault length between blocks 1 and 2 and the maximum overlap between blocks reaches 10% of the block width between blocks 3 and 4.

In the minimum strain strategy for restoring the same map, a continuum model of the map surface is first generated (Fig. 7d). This model honors the fault gap geometry and topology as it is mapped, such that terminating faults actually terminate in the model. The algorithm then analyzes the fault gap topology to make initial contact constraint assignments (Fig. 7e). During reconstruction, the contact assignments are updated between iterations. A restored configuration is found that closes the fault gaps without overlaps or gaps, with a minimum shear strain of the map surface (Fig. 7f). In this reconstruction, there is no slip beyond the fault terminations and there is no overlap or gap between fault blocks, to within arithmetic precession. The shear strain within the map surface needed to close the fault gaps averages 10% and reaches 50% in small regions near either end of the fault between blocks 3 and 4. The corresponding bulk strain, or change in surface area, averages 0.16% over the map surface.

5.2. Cylindrical fold

We test the extent to which the algorithm described in

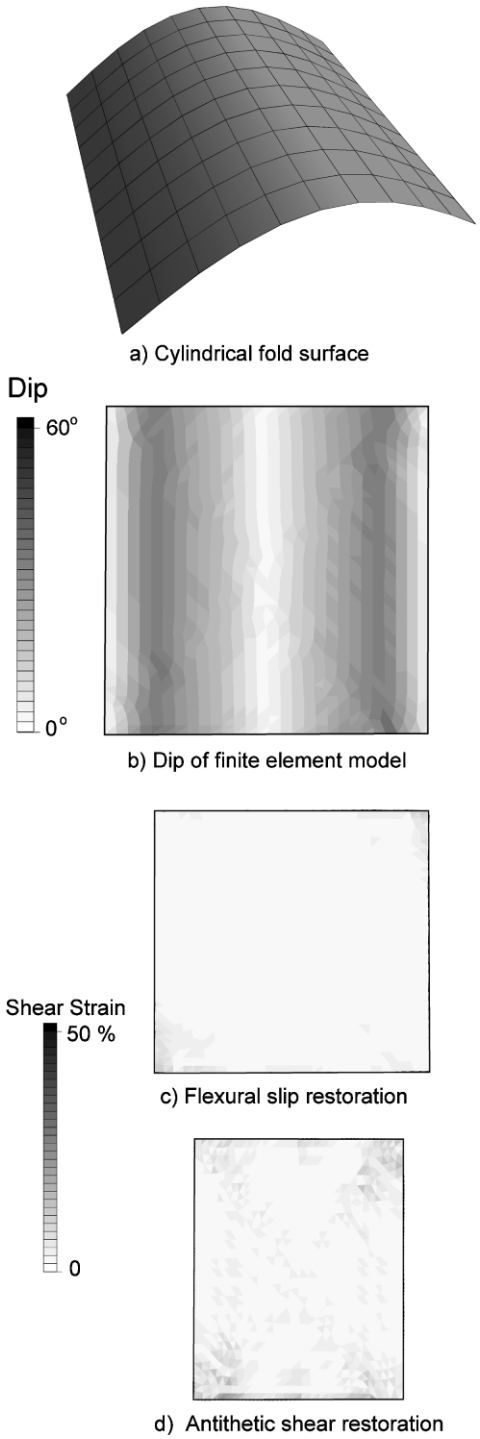

Fig. 8. Cylindrical fold synthetic example. (a) Cylindrical fold defined by a sine function from 0 to 180°. (b) Dip of the surface of the initial finite element model of the cylindrical fold. (c) Minimum residual strain reconstruction of the cylindrical fold assuming a flexural slip deformation mechanism. The residual shear strain averages 0.7% and the bulk strain average 0.08%. (d) Minimum residual strain reconstruction of the cylindrical fold assuming an antithetic shear mechanism oriented 60° from the vertical in the direction parallel to the local dip. The residual shear strain averages 1.8% and the bulk strain averages 0.07%.

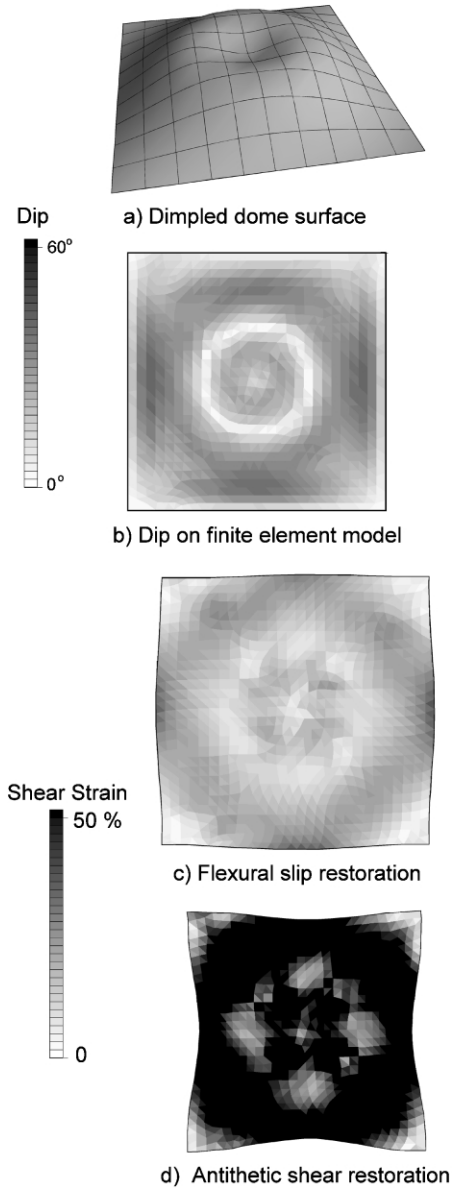

Fig. 9. Non-cylindrical fold synthetic example. (a) Non-cylindrical fold in the form of a dimpled dome. (b) Dip of the surface of the initial finite element model of the non-cylindrical fold. (c) Minimum residual strain reconstruction of the non-cylindrical fold assuming a flexural slip deformation mechanism. The residual shear strain averages 0.15% and the bulk strain average 0.24%. (d) Minimum residual strain reconstruction of the non-cylindrical fold assuming an antithetic shear mechanism oriented 60° from the vertical in the direction parallel to the local dip. The residual shear strain averages 57% and the bulk strain averages 0.53%.

this paper can find a true minimum strain solution by using it to flatten a cylindrical fold (Fig. 8). In principle, cylindrical folds in surfaces can be flattened without strain. Hence, the minimum strain reconstruction of a cylindrical fold should result in no shear or bulk strain. For this test, we generated a surface that varies as sine, from 0 to 180° over the distance of 1000 units in the x direction, is constant for 1000 units in the y direction, and reaches a peak height of 200 units in the z direction (Fig. 8a). We sampled this function to produce a square grid of 11 × 11 control points, which were imported

into the map reconstruction program. Variation in the dip along strike in the associated finite element model surface shows a small level of deviation from a true cylindrical surface (Fig. 8b). The restoration of the surface is done assuming flexural slip (Fig. 8c) and antithetic shear oriented at 60° in the direction of the local dip (Fig. 8d). Both mechanisms should unfold the surface without additional strain. Instead, the reconstruction by flexural slip requires an average residual shear strain of 0.7% and an average bulk strain of 0.08%. The antithetic shear mechanism results in an average residual shear strain of 1.8% and an average bulk strain of 0.07%. In both cases, part of this error is associated with non-cylindrical imperfections in the initial model surface and part is due to error in the finite arithmetic precision with which the nonlinear system of equations is solved. Both sources of error could be reduced to arbitrarily small levels by decreasing the element size and increasing the arithmetic precision of the solution, but at a cost of increasing solution time. However, in practice, this level of error is typically small relative to the uncertainty in the mapping of real structures.

5.3. Non-cylindrical fold

The goal of the minimum strain reconstruction is to flatten folds with the least additional shear strain, while preserving the area prescribed by the assumed deformation mechanism. The previous example shows that the bulk strain can be limited to less than 0.1% on average for a surface that requires no shear strain to reconstruct. In this last synthetic example, we test the accuracy with which area can be preserved for a case in which significant shear strain is required to flatten the surface. Following Rouby et al. (2000), we choose a dimpled dome as a test surface that cannot be formed without strain (Fig. 9a). We first generate a finite element model of this surface (Fig. 9b). Then, as in the previous example, we flatten the model surface assuming flexural slip (Fig. 9c) and 60° antithetic shear (Fig. 9d). The flexural slip deformation mechanism implies conservation of line length in cross-section and conservation of bed area in map view. The reconstruction of the test surface assuming flexural slip requires an average shear strain of 15% and an average bulk strain of 0.24%. The comparable reconstruction assuming 60° antithetic shear results in an average shear strain of 57% and an average bulk strain of 0.53%. Hence, area can be constrained to that prescribed by the assumed strain mechanism to well within 1%, for surfaces requiring high residual shear strain levels for the reconstruction.

6. Field examples

6.1. Complex fault gap topology

We also apply the new map reconstruction method described in the preceding sections to three subsurface structure maps (Figs. 10–12). The first is a reconstruction of the map used to illustrate the model building process (Fig. 1). It provides examples of complexities that arise in structure maps and their treatment in map reconstruction. The map contains numerous faults that terminate within the map and branch in complex ways as well as examples of faulted faults. The restored elemental configuration generated using the vertical simple shear assumption closes the fault gaps with a minimum distortion of the vertically projected triangle shapes (Fig. 10a). Displacement vectors between the present-day and restored nodal positions indicate a largely radial opening about the central region of the map (Fig. 10b). In the northeast quadrant of the map, the radial opening was accomplished by faulting. Elsewhere, the motion appears to have occurred through continuum strain. A high average residual strain level of 23% and concentrations in excess of 50% near fault tips indicate problems with the fault-gap geometry as it is mapped.

6.2. Global versus sequential restoration

The second example illustrates solution order artifacts that can occur in reconstructions in which fault blocks are restored serially, rather than as part of a global optimization (Fig. 11). Fig.11b shows a reconstruction in which four separate fault blocks around a salt dome are restored serially, as is the practice in previously described map reconstruction methods. Initially, a minimum residual strain solution is found for block 1 alone. Then another minimum strain solution is found for block 2, in which block 2 is required to fit against the restored block 1. This is repeated for block 3 and then block 4 is required to fit into the remaining space between blocks 1 and 3. Because error accumulates with each block, there is insufficient space left for block 4 and high residual strains result in that block. In the corresponding reconstruction of the same map, in which residual strain is minimized globally, no high residual strain levels occur (Fig. 11c).

6.3. Different shear deformation mechanisms

In a third example, a rollover anticline within the hanging wall of a major normal fault detachment in South Texas is used to illustrate the effect of different assumed strain mechanisms (Fig. 12). Reconstruction assuming vertical simple shear preserves the vertical projection of the map surface area (Fig. 12b). Bed-parallel shear (flexural slip) preserves the three-dimensional map surface area (Fig. 12c). Antithetic shear, inclined 67° from horizontal in the direction counter to the local dip, decreases the map surface area by a variable amount depending on the magnitude of the local dip (Fig. 12d). Overall, the vertical simple shear assumption results in the smallest average residual strain (5%). However, the reconstruction assuming bed-parallel

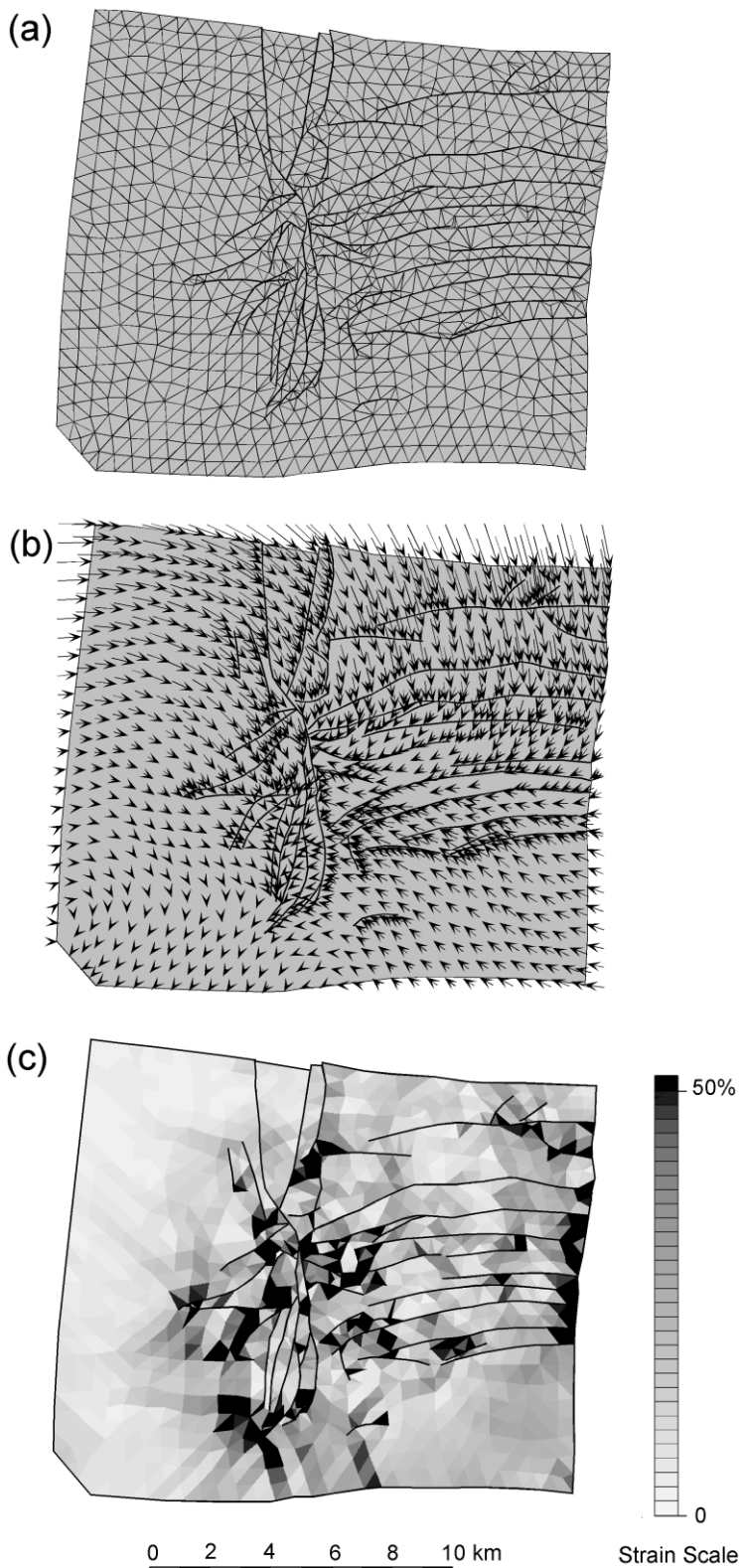

Fig. 10. Reconstruction of a faulted and folded horizon. (a) Restored element configuration of the map shown in Fig. 1, assuming a vertical simple shear deformation mechanism. (b) Displacement vector pattern between the present-day nodal positions (vector tails) and the restored nodal positions (vector heads). (c) Distribution of residual strain. This display shows the heterogeneous strain required to close the fault gaps, beyond that involved in the vertical simple shear of the elements to the horizontal plane.

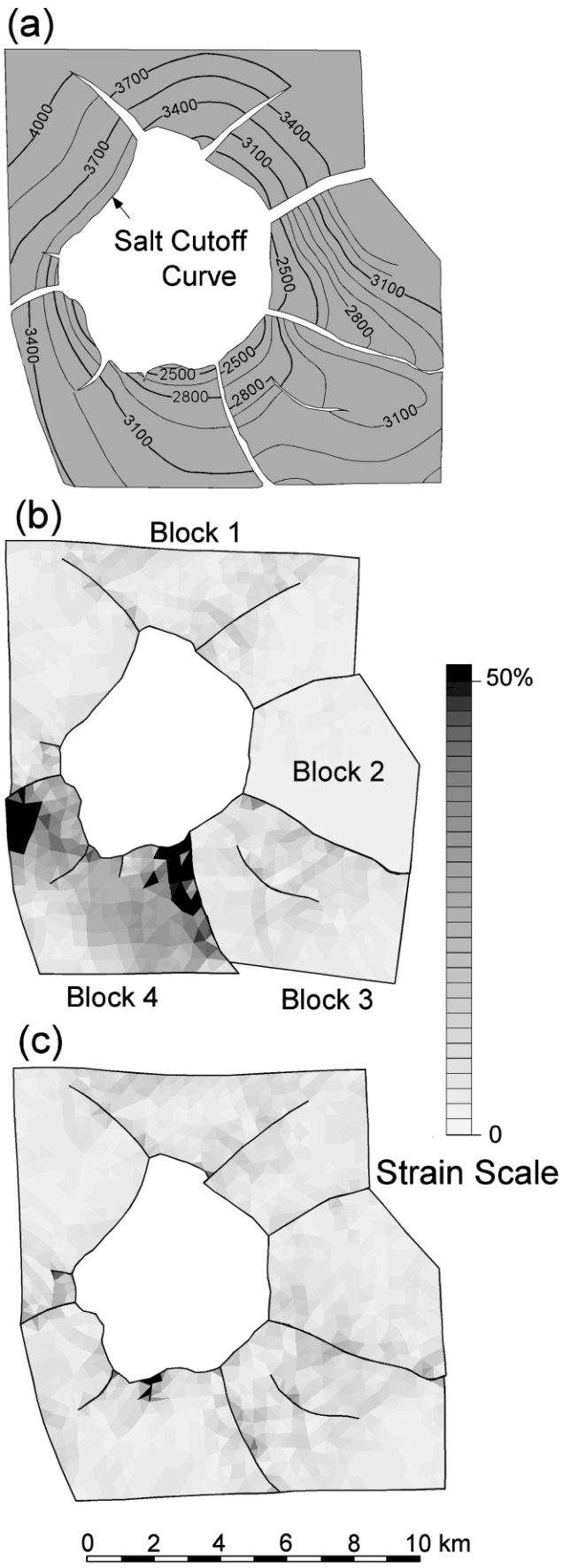

shear produces lower levels of residual strain in the gently dipping southeastern flank of the anticline. One possible explanation is that much of the dip within the southeastern flank formed by bed rotation, rather than by continuum shear deformation. The antithetic shear assumption produces lower residual strain concentrations in the northwest flank of the anticline. One possible explanation is that there was a component of continuum strain or sub-seismic antithetic faulting, down thrown to the northwest, within the northwestern limb of the anticline. Hence, in this case vertical simple shear results in the least overall strain. However, different strain mechanisms may provide a closer approximation to the true geologic strain in different parts of the structure. This illustrates the potential pitfall of trying to determine true geologic deformation through reconstruction methods. The deformation mechanism that results in the 'best' reconstruction in a least strain sense need not be the closest to the true geologic strain. In practice, it is better to assign deformation mechanisms through direct examination of the rocks where possible and from general knowledge about how rocks deform in analogous tectonic setting where direct observation is not possible. These different strain mechanisms can then be assigned on an element, fault block or map wide basis.

7. Discussion

All kinematic reconstruction methods, including the one described in this paper, are merely tools by which geologists can test to see if their ideas about the geometry of a structure are consistent with their ideas about the kinematics of its formation. The results are inherently non-unique and do not prove that a particular structural interpretation is correct. It is quite possible for interpretations to reconstruct well and still contain significant geometric errors. For example, an unfaulted, horizontal plane is not the correct geometry for any of the field examples given in this paper and yet such a map reconstructs perfectly, regardless of the deformation mechanism assumed. Conversely, interpretations that reconstruct poorly do not necessarily contain geometric errors. All that can be stated with certainty about interpretations that reconstruct poorly is that the interpreted geometry is inconsistent with the assigned kinematics. The

Fig. 11. Solution order artifacts for the reconstruction of a faulted horizon surrounding a salt dome. (a) Present-day configuration of the top of the Grand Isle Ash, Grand Isle Block 16 Field, Offshore Louisiana, modified from Tearpock and Bischke (1991, Fig. 8-71). Depth contours are in meters. The map surface is artificially divided into four separate fault blocks by faults that extend from the salt-sediment interface to the map edge. (b) When reconstructed one block at a time, position error accumulates with each block. The last block restored (fault block 4) requires high levels of residual strain to fit into the remaining space between blocks 1 and 3. (c) The map restores with little residual strain, if all blocks are restored simultaneously and the residual strain is minimized globally.

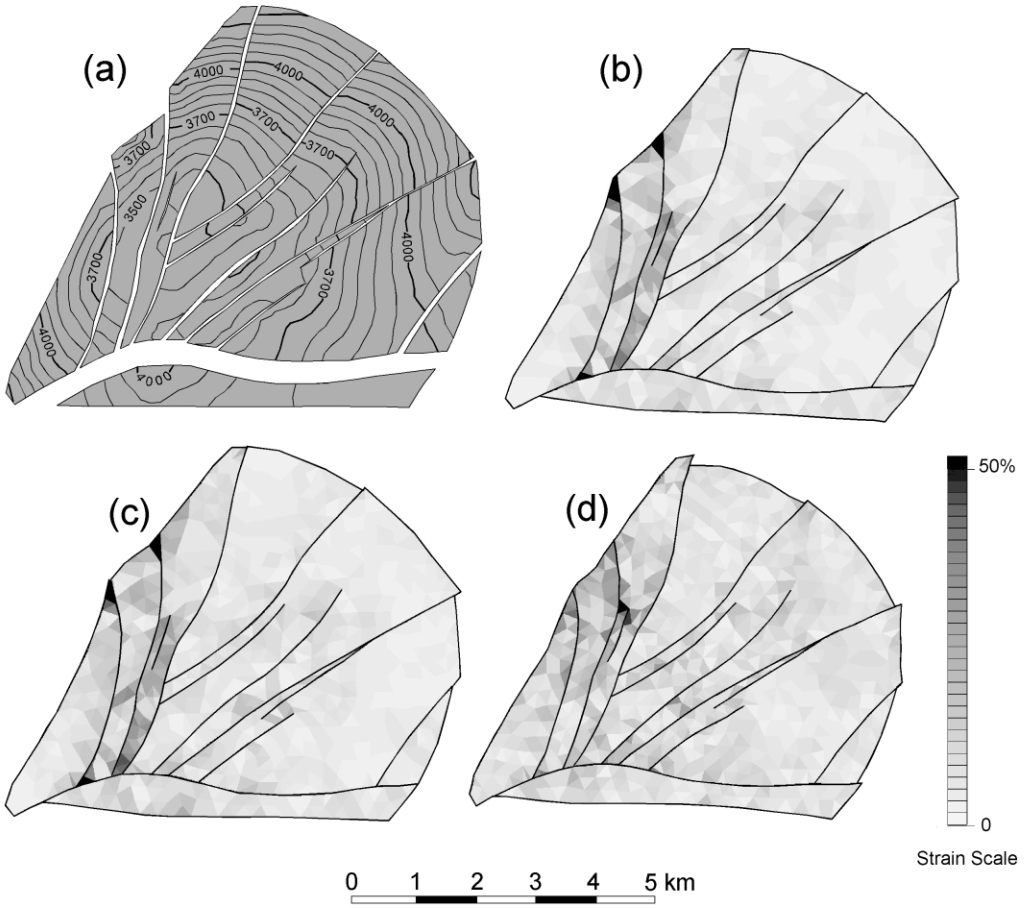

Fig. 12. Map reconstructions with different homogenous strain mechanisms. (a) Structure map from a mature South Texas gas field based on closely spaced well control and two-dimensional seismic profiles. Depth contours are in meters. (b) Map reconstruction assuming vertical simple shear. The residual strain averages 5% over the map surface. Peak residual strains in excess of 50% occur near branches between antithetic faults and the main detachment fault. (c) Map reconstruction assuming a bed-parallel slip deformation mechanism. The residual reconstruction strain averages 7% over the map surface. Residual strain levels are lower than those for vertical simple shear in the gently dipping southeast limb and higher in the more steeply dipping northwest limb. (d) Map reconstruction assuming simple shear inclined 67° antithetic to the local horizon dip. The average residual strain of 8% is slightly higher than for both vertical simple shear and bed-parallel shear, but the areas of high peak strain in the northwest limb are eliminated.

problem may lie in the geometry, it may lie in the assigned deformation mechanisms, or the problem may be caused by a combination of errors in both. The value of reconstructions is that the process of doing the reconstruction can identify such inconsistencies.

Different reconstruction strategies have different levels of sensitivity to various kinds of map errors. We rigorously constrain the local map area to that prescribed by the selected deformation mechanism and prevent all overlap and gap between fault blocks. Hence, our approach is more sensitive than other methods to mapping errors that result in either excess or missing map surface area. These types of errors commonly occur in two ways in maps produced from three-dimensional seismic interpretations. Because the terminations of horizons at fault-horizon intersections are difficult to image precisely, the exact position of horizon cutoff curves is difficult to map directly. This can result in mapping errors in which the fault gaps are either too large, meaning that locally there is missing map area, or too small, meaning that locally there is excess map area. Another common problem in interpreting seismic data is correlating across faults into isolated fault blocks with no well control. It is easy to miscorrelate to a seismic loop above or below the correct surface. These correlation errors result in isolated fault blocks that are either too large or too small to fit into the space left by the surrounding blocks. Both of these types of errors have important practical implications. In the first case, it is common to target production wells as high up dip and as close to a production-limiting fault as possible. Errors in the size of the fault gap jeopardize such wells. In the second case, errors in fault block area translate directly into errors in fluid volume calculations. In reconstructions made by methods less sensitive to errors in map area, such problems may go unnoticed.

The map reconstruction method described in this paper offers at least five other advantages over previously proposed methods:

(1) The new method more faithfully honors the user's interpretation and subjects it to a more rigorous test

than previous methods. Previously proposed map reconstruction methods do not explicitly treat complex fault gap networks, with terminating faults and different kinds of branch points. The occurrence of fault tips and antithetic and synthetic fault branches have important kinematic implications for the formation and reconstruction of faulted surfaces. Instead of treating these features explicitly, previous methods artificially subdivide such networks into individual fault blocks that can move independently (Barr, 1985; Gratier et al., 1991; Gratier and Guiller, 1993; Rouby et al., 1993, 2000). As a result, many of the kinematic implications of a particular interpretation are lost and go untested.

(2) In the new method all reconstruction error is, to numerical precision, manifest in the amplitude of a single parameter, the residual shear strain. We chose this approach because it is known with certainty that unfaulted regions of the map in the present should be unfaulted in the initial state and that there should be no overlaps or gaps between fault blocks. Similarly, large changes in rock volume beyond that associated with compaction are seldom expected. However, some amount of shear strain beyond that imparted by simple deformation mechanisms is geologically reasonable. We do not propose the minimum strain criterion as a rule by which the actual distribution of rock strain can be determined. Instead, we use this criterion as a measure of the extent to which the true rock strain can be explained using the particular idealized deformation mechanisms assigned by the user. This approach makes it possible to quantitatively compare reconstructions of slightly different interpretations of the same structure.

In previous reconstruction methods, all kinematic constraints are enforced by least squares fit and none is necessarily enforced to high precision, except by chance. Hence, reconstruction error can be manifest as local area change that differs from that implied by the chosen deformation mechanism, as slip beyond fault tips, and as overlap and gap between fault blocks. This leads to problems such as having to compare a reconstruction that results in a large change in area, but has little overlap and gap between fault blocks, with another reconstruction that produces less area change but more overlap and gap between fault blocks. Under these conditions, the question of which is the better reconstruction is ambiguous.

(3) The new method finds a global solution to the reconstruction problem in which unfolding and unfaulting of all map regions occurs simultaneously as one step. In this way, a solution is found that honors all the kinematic conditions with equal weight. Previous approaches have all resorted to treating parts of the problem in sequence. The treatment order imparts an unintended weighting of kinematic constraints. As a result, there is greater freedom to fit parts of the model treated earlier in the sequence than those treated later in the sequence. A disproportionate amount of reconstruction error tends to be concentrated in the parts of the model treated last, regardless of where the problem lies. In many cases, such solution order artifacts are insignificant, particularly in cases in which there is a dominant direction of motion. However, maps of truly three-dimensional structures can seldom be restored without exhibiting solution order problems to some extent. This is particularly true in cases in which the geometry forces the last piece treated to be restored against the first piece treated, such as in example 6.2.

(4) In the new method the reconstruction process is fully automated. This is possible because the underlying geometric models faithfully reproduce the topology of the horizon map. Special attention is paid to the topology of the cutoff curve network. Cutoff curves associated with through-going surfaces that are intersected by other terminating surfaces are represented as curves with multiple disconnected segments. The kinematic significance of the end points of these segments, whether fixed branch, sliding branch or tip, is determined automatically from the characteristics of connecting curve segments. All that is required is that the horizon-cutoff curve network be digitized and labeled in a manner consistent with the true topology of the intersecting surfaces. The reconstruction can then be performed without further manual manipulation. This greatly reduces the labor involved in reconstructing complexly faulted horizons. However, the most important advantage is that the reconstructions are reproducible. Once the initial model is constructed, it can be restored any number of times with the same result. This makes it possible to perform reconstructions with different assigned strain mechanisms or modified geometry with the assurance that the only differences in the restorations are associated with the changes in the initial model and constraints (Fig. 12). In methods in which fault blocks are fitted by manual manipulation, differences in the placement of fault blocks on repeated reconstruction produce different results from the same starting configuration.

(5) The finite element formation used in the described map reconstruction method is general in nature and extends to other dimensions in a straight forward way. The method we describe in this paper is the middle of three reconstruction applications developed using the same approach. The first was a cross-section reconstruction application that has been used on a proprietary basis for over a decade. A full three-dimensional algorithm has also been developed, in which many of the same topological and kinematic rules described for map

reconstruction apply. However, rock masses are represented by volume elements rather than the surface elements used in map reconstruction and fault contact is maintained between fault surfaces rather than between cutoff curves. Experience using the three applications has shown that the four previously described advantages of the minimum strain formulation are of some importance in cross-section reconstruction, but are of greater importance in map reconstruction. However, in the three-dimensional reconstruction application these advantages became critical. In practice, having the three-dimensional reconstruction capability is seldom useful unless the true topology of the fault network is treated explicitly, a global solution is found, error is restricted to one parameter, and the reconstruction process is automated. We reserve a description of three-dimensional minimum residual strain reconstruction for a future paper.

8. Conclusion

In this paper, we describe a finite element method for palinspastic reconstruction of faulted and folded horizon maps. Map surfaces are represented by finite element models with the same geometry and topology as the faulted horizons. During model construction, geometric and topological rules are used to automatically identify initial conjugate points and conjugate cutoff curves between fault blocks. This allows the reconstruction to proceed without manual manipulation. To the extent possible, horizon deformation is removed assuming deformation mechanisms and kinematic constraints used in conventional structural reconstructions. The component of residual strain required to flatten folds and close fault gaps is found by solving the global optimization problem in which map surface is treated as a hyperelastic membrane. The use of a hyperelastic membrane constitutive model guarantees the minimum total residual strain with the smoothest possible distribution required to satisfy the kinematic constraints. The main advantages of this approach over those previously described are that faults that terminate within the mapped regions and non-cylindrical folding can be explicitly treated, and artifacts associated with sequential restoration of fault blocks are avoided.

Acknowledgements

The map reconstruction algorithm presented in this paper was developed at Shell Technology Company in the early 1990s as a team effort. We specifically acknowledge the contributions of Charlie Harvey and Fred Diegle, who helped conceive and shape the ideas presented. Steve Tennant of Shell made the map used as example 7.3. The original manuscript was substantially improved as the result of suggestions of reviewers Shankar Mintra and Frank Bilotti. We also thank Shell International Oil Company for permission to publish the work.

References

Barr, D., 1985. 3-D palinspastic restoration of normal faults in the Inner Moray Firth: implications for extensional basin development. Earth and Planetary Science Letters 75, 191–203.

Becker, E.B., Carey, G.F., Oden, J.T., 1981. Finite Elements An Introduction, Prentice-Hall, Englewood Cliffs, NJ.

Dahlstrom, C.D.A., 1969. Balanced cross-sections. Canadian Journal of Earth Science 6, 743–757.

Deljouie-Rakhshandeh, K., 1990. An approach to the generation of triangular grids possessing few obtuse triangles. International Journal for Numerical Methods in Engineering 29, 1299–1321.

Dhatt, G., Touzot, G., 1984. The Finite Element Method Displayed (G. Cantin, Trans.). John Wiley and Sons, New York (original work published 1983).

Erickson, S.G., Hardy, S., Suppe, J., 2000. Sequential restoration and unstraining of structural cross-sections: applications to extensional terranes. American Association of Petroleum Geologists Bulletin 84, 234–249.

Fletcher, R., 1987. Practical Methods of Optimization, 2nd Ed, John Wiley and Sons, New York, 436pp.

Fried, I., Johnson, A.R., 1988. A note on elastic energy density function for largely deformed compressible rubber solids. Computer Methods in Applied Mechanics and Engineering 69, 53–64.

Gibbs, A.D., 1983. Balanced cross-section construction from seismic sections in areas of extensional tectonics. Journal of Structural Geology 5, 153–160.

Gratier, J.P., Guiller, B., 1993. Compatibility constraints on folded and faulted strata and calculation of total displacement using computational restoration (UNFOLD program). Journal of Structural Geology 15, 391–402.

Gratier, J.P., Guiller, B., Delorme, A., 1991. Restoration and balance of a folded and faulted surface by best-fitting of finite elements: principles and applications. Journal of Structural Geology 13, 111–115.

Green, P.J., Sibson, R., 1978. Computing Dirichlet tessellations in the plane. The Computer Journal 21, 168–173.

Gruttmann, F., Taylor, R.L., 1992. Theory and finite element formulation of rubberlike membrane shells using principal stretches. International Journal for Numerical Methods in Engineering 35, 1111–1126.

Jin, H., Wiberg, N.E., 1990. Two-dimensional mesh generation, adaptive remeshing and refinement. International Journal for Numerical Methods in Engineering 29, 1501–1526.

Morretti, I., Larrere, M., 1989. LOCACE: computer-aided construction of balanced geological cross-sections. Geobyte 4, 16–24.

Rouby, D., Cobbold, P.R., Szatmari, P., Demercian, S., Coelho, D., Rici, J.A., 1993. Restoration in plan view of faulted Upper Cretaceous and Oligocene horizons and its bearing on the history of salt tectonics in the Campos Basin (Brazil). Tectonophysics 228, 435–445.

Rouby, D., Xiao, H., Suppe, J., 2000. 3-D restoration of complexly folded and faulted surfaces using multiple unfolding mechanisms. AAPG Bulletin 84, 805–829.

Rowan, M.G., Kligfield, R., 1989. Cross-section restoration and balancing as and aid to seismic interpretation in extensional terranes. The American Association of Petroleum Geologists Bulletin 73, 955–966.

Schultz-Ela, D.D., 1991. Practical restoration of extensional cross-sections. Geobyte 6, 14–23.

Simo, J.C., Taylor, R.L., 1982. Penalty function formulations for

incompressible nonlinear elastostatics. Computer Methods in Applied Mechanics and Engineering 35, 107–108.

Tearpock, D.J., Bischke, R.E., 1991. Applied Subsurface Geological Mapping, Prentice Hall PTR, Upper Saddle River, NJ, 646pp.

Worrall, D.M., Snelson, S., 1989. Evolution of the northern Gulf of Mexico, with emphasis on Cenozoic growth faulting and the role of salt. In: Bally, A.W., Palmer, A.R. (Eds.), The Geology of North America—An Overview. Geological Society of America, Boulder CO, A, pp. 97–138.